J Mater Sci (2019) 54:10437–10446

Materials for life sciences

3D printing of bioglass-reinforced β-TCP porous bioceramic scaffolds

Yule Ma[1], Honglian Dai[1,2,*], Xiaolong Huang[1], and Yanpiao Long[1]

[1] State Key Laboratory of Advanced Technology for Materials Synthesis and Processing, Wuhan University of Technology, Wuhan 430070, Hubei, People's Republic of China

[2] Biomedical Materials and Engineering Research Center of Hubei Province, Wuhan 430070, People's Republic of China

Received: 22 February 2019
Accepted: 15 April 2019
Published online: 23 April 2019

ABSTRACT

The use of bioglass (BG) has been proved to be an effective strategy for reducing the sintering temperature and improving the degradability of bioceramics. In this work, a Na_2O–CaO–MgO–P_2O_5 bioglass with a low melting temperature and an average particle size of 1.3 μm and crystalline β-tricalcium phosphate (β-TCP) with an average particle size of 600 nm were first prepared separately. 3D printing was then used to fabricate the β-TCP/BG composite porous ceramic scaffolds. The Na_2O–CaO–MgO–P_2O_5 bioglass-reinforced β-TCP porous ceramic scaffolds demonstrated a significant enhancement in their mechanical properties, degradability and biocompatibility compared with pure β-TCP ceramics. The results showed that the compressive strength and elastic modulus of the reinforced β-TCP ceramic scaffold were 8.34 MPa and 208.5 MPa, respectively, and the degradation rate of the β-TCP porous ceramic scaffolds increased by a factor of 2.99. In addition, the optimized scaffold distinctly promoted MC3T3-E1 osteoblast cell proliferation. Na_2O–CaO–MgO–P_2O_5 bioglass-reinforced β-TCP porous ceramic scaffold has great potential for application in bone regeneration.

Introduction

In addition to the 'gold standard' autologous bone grafts [1], tissue engineering has been considered one of the most effective strategies for regenerating and restoring tissue damaged by illness, accidents or tumor excision [2]. Generally, in the field of bone tissue engineering, the biocompatibility, mechanical properties and capacity for tissue regeneration of scaffolds should be taken into consideration first [3]. Additionally, high porosity and interconnected porous structures with an appropriate pore size (100–400 μm) are of great importance for allowing osteoconduction, vascularization and the transport of nutrients and metabolic wastes [4–7].

Calcium phosphate-based bioceramics exhibit excellent biocompatibility, bioactivity and osseointegration properties because their composition is similar to that of bones, which consist of hydroxyapatite (HA), tricalcium phosphate (TCP) and biphasic calcium phosphate (BCP) [6, 8–13]. In particular, β-TCP

Address correspondence to E-mail: daihonglian@whut.edu.cn

https://doi.org/10.1007/s10853-019-03632-3

(β-$Ca_3(PO_4)_2$), a low-temperature-stable phase of TCP, was considered to be degradable [14] and osteoconductive [15]. It has been the subject of extensive and long-term research for use as a bone graft substitute [16–18]. However, as an essential factor for biomaterials [19, 20], β-TCP was reported to have a degradation rate of 2.3% in vitro over 5 weeks [21] and could barely be resorbed in vivo after 6 months [22]. Degradation is an important factor for biomaterials [21, 22]. Furthermore, Na_2O–CaO–P_2O_5–SiO_2 series bioglasses can effectively reduce the sintering temperature, improve biological activity and enhance the degradability of bioceramics [23–27]. Magnesium-doped Na_2O–CaO–P_2O_5 bioglass showed improved bioactivity and biocompatibility when compared with non-doped one [28].

In addition, with conventional methods for the preparation of porous bioceramics, such as porogen [29], gel-polymer processes [30] and slip-casting [31], it is quite difficult to control the pore size and interconnected pore structure [32]. In recent years, the emergence of rapid fabrication technology has showed promise in addressing this problem. Many studies have been carried out using 3D printing technology to prepare various scaffold materials with high porosity and customizable pore sizes [33–37]. A PCL/β-TCP composite scaffold was obtained by melt-extrusion with easy pore shape and size control [38]. A calcium phosphate porous bioceramic scaffold with a perfect pore structure and a porosity of 55% was prepared by inkjet 3D printing technology [39].

In this paper, ultrafine Na_2O–CaO–MgO–P_2O_5 bioglass powder and ultrafine β-TCP powder were prepared by melting and coprecipitation, respectively. The β-TCP/BG composite porous ceramic scaffolds were successfully fabricated by 3D printing equipment. The effect of bioglass on the biocompatibility, mechanical properties and degradability of the β-TCP scaffold were studied in detail.

Materials and methods

Synthesis of β-TCP and Na_2O–CaO–MgO–P_2O_5 BG superfine powders

Samples of pure β-TCP were prepared by the coprecipitation method as reported previously. Briefly, 141.69 g $Ca(NO_3)_2{\cdot}4H_2O$ was dissolved in 1200 mL deionized water, and 52.8224 g $(NH_4)_2HPO_4$ was dissolved in 800 mL deionized water, and then, a calcium solution was added dropwise to the phosphate solution over 4 h with stirring. During coprecipitation, the pH value was maintained at 7.0. After aging for 24 h, the suspension was filtered and dried at 110 °C. Finally, after heating at a rate of 10 °C/min, the obtained powders were calcined at 800 °C for 2 h.

Na_2O–CaO–MgO–P_2O_5 bioactive glass was prepared by the melting method. Na_2CO_3, $CaCO_3$, $(MgCO_3)_4{\cdot}Mg(OH)_2{\cdot}5H_2O$ and $NH_4H_2PO_4$ were weighed according to the weight percentage of 18 wt% Na_2O, 10 wt% CaO, 7 wt% MgO, 65 wt% P_2O_5. Deionized water was added as the solvent. The mixture was heated and stirred to remove NH_3 and then transferred to a crucible and melted at 900 °C. After a refining period, the melt was poured into water for quenching. The obtained BG was ground in ethanol using zirconia balls for 6 h.

All of the chemical reagents used in this study were purchased from Sinopharm Chemical Reagent Co., Ltd. (China).

Ceramic ink writing of β-TCP/BG scaffolds

β-TCP powders with BG contents of 5 wt%, 10 wt%, 15 wt% and 20 wt% were thoroughly mixed via ball milling and dried at 60 °C for 24 h. To prepare the injectable ink, 44 g β-TCP/BG powders, 18 g sodium alginate suspension (10 wt%), 5 g Pluronics F-127 solution (20 wt%) and 6 ml deionized water were mixed by milling. After homogeneous mixing, the inks were placed into printing tubes, and 1.5 ~ 2.5 bar nitrogen pressure was applied. The scaffolds were generated using a homemade 3D printing equipment at a moving speed of 3 mm/s and were dried at room temperature for 24 h and sintered at 710 °C for 2 h. As a control, due to the poor sintering effect under 710 °C, pure β-TCP scaffolds prepared by the same method (marked as S1) were sintered at 1100 °C for 2 h at a heating rate of 10 °C/min as reported previously [40]. The β-TCP/BG20 scaffold sintered at 800 °C for 0.5 h was labeled as S2.

Characterization of β-TCP and BG powders

The crystal phases of the β-TCP and milled BG powders were determined by an X-ray diffractometer (XRD, D8 Advance, Bruker Co., Germany) using Cu Kα radiation and operating at 40 kV with 40 mA current. The 2θ angle data were obtained in the range

of 10°–65° at a scanning speed of 5.0 degrees/min. The morphology of the β-TCP and BG powders was observed by using a Zeiss Ultra Plus field emission scanning electron microscope (ULTRA plus FESEM, Zeiss, Germany). Thermogravimetric and differential scanning calorimetry (TG-DSC) curves of the BG powders and β-TCP/BG20 raw scaffold were tested by a thermal analysis-mass spectrometer (DSC8500, Perkin Elmer, USA). The particle size distribution of β-TCP and BG powders was determined by dynamic light scattering (DLS, Mastersizer 2000, Malvern Instruments Ltd., UK).

Characterization and mechanical properties of the scaffolds

SEM was used to observe the scaffolds' morphology and pore structure and the internal micropore structure of the filament. Cubic scaffolds (10 × 10 × 10) were fabricated for compressive strength measurements that were performed by a universal testing machine (MTS, America) at a cross head displacement rate of 0.5 mm/min. To obtain average values, the mechanical strength was measured for five scaffolds per group. XRD (XRD, D8 Advance, Bruker Co., Germany) was used to analyze the phase composition of the β-TCP/BG scaffolds after sintering and degradation.

Degradation property of the scaffolds

The degradation property of the scaffolds was evaluated by using Tris–HCl (pH 7.40) as the buffer solution. The scaffolds were soaked for different time periods at 37 °C. Tris–HCl solution was added 200 mL/g relative to the mass of the scaffold. After soaking for 1, 3, 7, 10, 14, 21 and 35 days, an electrolyte-type pH meter (PHS-3C, Jinke Leici Co., Shanghai, China) was used to measure the pH values of the solution without refreshing the immersion medium. After soaking, the final weight of each scaffold sample was measured precisely after drying at 110 °C for 1 day. The percentage relative to the initial weight was shown as the weight loss.

Cell proliferation assay

The MTT assay was used to determine the cell viability. The culture medium (a-MEM medium, HyClone, USA) containing mouse preosteoblast cells (MC3T3-E1, American Tissue Type Collection HTB96) was exposed to the porous scaffolds for each sample and supplemented with 10% fetal bovine serum and 1% penicillin/streptomycin for 1, 3 and 5 days and cultured at 37 °C in a humidified incubator with 5% CO_2; then, 10 μL of 3-[4,5-dimethylthiazol-2-yl]-2,5-diphenyltetrazolium bromide (MTT, 5 mg/ml) was added to each well, and the cells were further cultured at 37 °C for 4 h [41]. The pure cells without culturing with scaffolds were used as the control. Then, a microplate reader (Multiskan GO, Thermo Scientific, USA) was used to measure the absorbance at 570 nm after the blue formazan crystals were dissolved in dimethyl sulfoxide (DMSO) that was generated by mitochondrial dehydrogenase in viable cells.

Statistical analysis

All of the data described above were expressed as the mean ± standard deviation (SD) and analyzed with one-way ANOVA. For all cases, a p value < 0.05 was considered statistically significant difference. The results were indicated with (*) for $p < 0.05$, (**) for $p < 0.01$.

Results and discussion

Characterization of β-TCP and BG powders

β-TCP powder was successfully prepared by the coprecipitation method, and Na_2O–CaO–MgO–P_2O_5 BG powder was produced by melting and milling posttreatment. The X-ray diffraction patterns of β-TCP and BG powders are shown in Fig. 1a, b, respectively. The β-TCP powder was a pure phase with high crystallinity (JCPDS card No. 09-0169), and the BG powder was amorphous. According to SEM observations, both the synthesized β-TCP powders and the as-milled BG powders were composed of superfine particles with diameters of less than 2 μm (Fig. 1c, d). The DLS results showed a narrow size distribution in the ranges of 300–1000 nm for β-TCP and 900–1500 nm for BG, respectively (Fig. 1e). The statistical analysis of the particle sizes obtained in the SEM images showed that the average particle size of the highly pure and highly crystalline β-TCP was 400 nm, and the average particle size of the bioglass with an irregular morphology was 750 nm (Fig. S1),

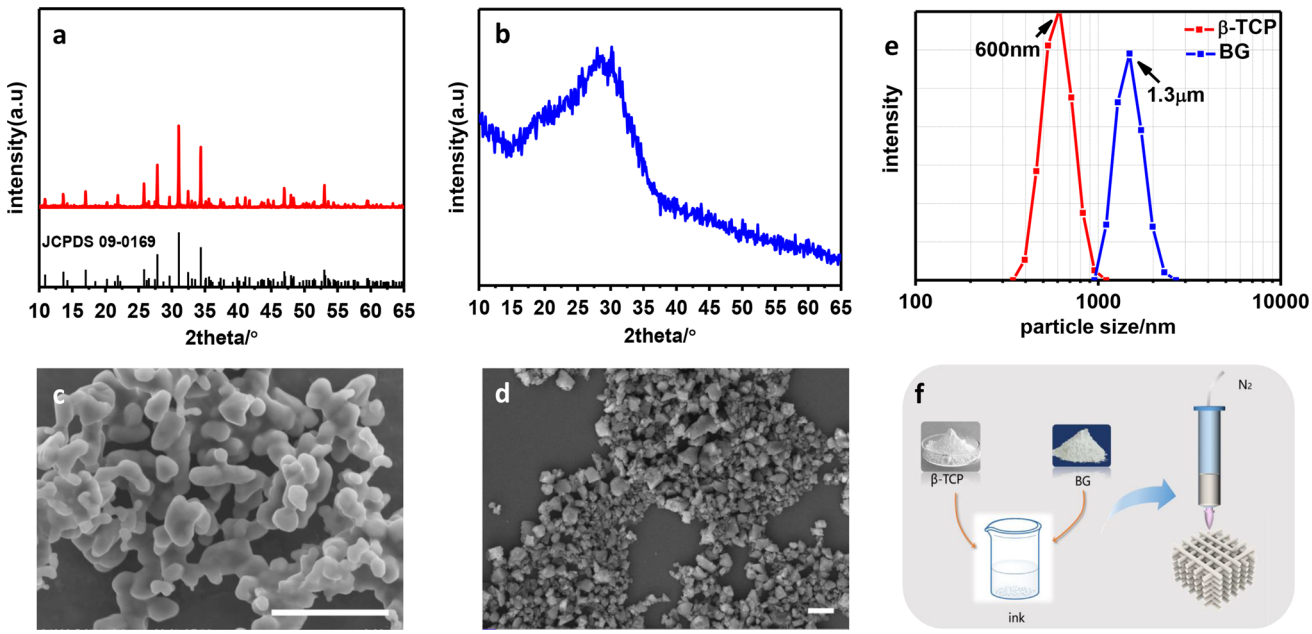

Figure 1 XRD patterns of β-TCP (**a**) and BG (**b**). SEM observation of β-TCP (**c**) and BG (**d**) particles (the scale bar represents 2 μm in both images). The particle size distribution was measured by DLS (**e**). The schematic diagram of this study (**f**).

consistent with the results of DLS analysis (Fig. 1e). Ultrafine particles have a large specific surface area and high reactivity [42, 43]. In this case, the β-TCP and BG particles were fully mixed and exhibited a large contact area that was beneficial to the interaction between the β-TCP and BG particles. In addition, the grains after sintering the ultrafine powders will exhibit good degradation activity due to the effect of their large specific surface area [44].

According to the DSC-TG curve presented in Fig. 2 and considering the endothermic/exothermic effect of the glass phase transformation during the melting procedure, it could be suggested that the glass transition temperature (T_g, endothermic effect) was in the range of 600–660 °C, the crystallization temperature (T_c, exothermic effect) was approximately 680–700 °C and the melting temperature (T_m, endothermic effect) was approximately 800 °C. In particular, the phase transition temperature range implied by the DSC-TG analysis of β-TCP/BG20% raw scaffold was roughly consistent with the above values (Fig. 2b). The exothermic peaks below 550 °C were due to the burning out of organic components. It should be noted that in the previous studies, the bioglass was generally added as a liquid phase sintering assistant to reduce the sintering temperature of ceramics and to reinforce the bioactivity [31]. Using this efficient sintering method, higher shrinkage and denser ceramics without microspore structure tend to be obtained. Fig. S2(a) shows the cross-sectional morphology of the β-TCP/BG20% scaffold sintered at 800 °C for 0.5 h that corroborated this trend. The results presented in the relevant literature showed that this dense sintering structure was not conducive to degradation and porosity [45]. The multiscale porous structure is thought to be helpful for new tissue regeneration [46]. Based on these considerations, 710 °C was selected as the sintering temperature in this study. In this case, the bioglass was proved to contribute a bonding effect and enhancement for the β-TCP grain.

Characterization of β-TCP-BG scaffolds

To build the porous β-TCP/BG composite scaffolds, we used sodium alginate gel and Pluronics F-127 as auxiliary additives to prepare a writing ink suitable for extrusion at room temperature using 3D printing equipment. By repeating the experiments and adjusting the formulation, we finally obtained several sets of inks for 3D printing, as listed in Table S1. The β-TCP/BG scaffolds with different shapes and sizes were fabricated with a pore size of 400 μm and a porosity of ~ 60%. To adjust the pore size and shape of ceramic scaffolds, we only need to adjust the STL design file and printing parameters,

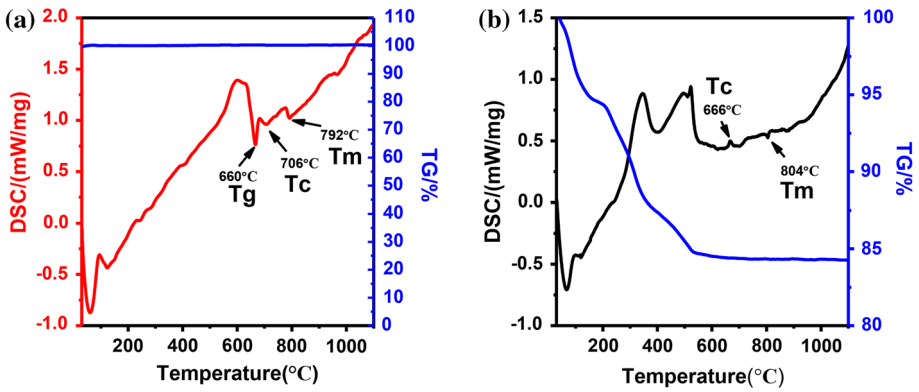

Figure 2 DSC-TG analysis of BG (**a**) and raw scaffold of β-TCP/BG20 (**b**). It was revealed that the Tg was in the range of 500–660 °C, the Tc was in the range of 666–706 °C, and the Tm was approximately 800 °C.

making it easy to meet the requirements of different bone defect models.

X-ray diffraction (XRD) was employed to investigate the effect of bioglass on the components of ceramic scaffolds. Figure 3 shows the XRD patterns of the β-TCP scaffolds with the addition of 5 wt%, 10 wt%, 15 wt% and 20 wt% bioglass after sintering. The results indicate that the diffraction peaks can be indexed to β-TCP (PDF#09-0169) and $Ca_2P_2O_7$ (PDF#09-0346). It is easily found that the peak intensity of $Ca_2P_2O_7$ increased with greater bioglass addition. As shown in Fig. 3b, a, magnified view of the diffraction curves shows that the (210) crystal plane shifted toward a larger angle with bioglass addition in the range of 5–20 wt%; this can be attributed to the partial replacement of the Ca^{2+} in β-TCP by the smaller Mg^{2+} and Na^{+} ions. The shift increased with increasing added glass content. This showed that bioglass reacted with β-TCP grains and became an integral part of the bioceramics.

The SEM images presented in Fig. 4 show the cross section micromorphology of the fabricated β-TCP/BG composite scaffolds that were sintered using a unified sintering schedule as described above. It is clear that with increasing bioglass addition, more bonding structures (indicated by white arrow in Fig. 4) and networks between β-TCP particles were obtained. By contrast, as shown in Fig. 4a, b, with less bioglass addition, the β-TCP particles in the cross section of the ceramic scaffolds accumulated independently of each other, lacking an effective integrally bonded mechanical structure. Moreover, it is clearly shown in Fig. 4 that the grain size of the β-TCP/BG20 scaffold was larger than that of β-TCP/BG5, and that the particle size of the latter one was much closer to that of primary β-TCP. This could be explained by the effect of the wetting and bonding of the bioglass on the β-TCP grain. This evidence illustrates the improvement of the micromechanical structure of the bioceramic scaffold due to bioglass.

It is important to note that there were no interconnected pores in the ceramic scaffolds and that only residual bubble pores were observed for the β-TCP/BG20 scaffold sintered at 800 °C for 0.5 h (S2) (Fig. S2a). The pure β-TCP scaffolds were sintered at 1100 °C for 2 h (Fig. S2b). High-temperature sintering results in grain boundary migration and excessive grain growth of β-TCP (up to 2 μm). This formation mechanism of the mechanical structure was different from that of the bioglass bonding effect. It appears

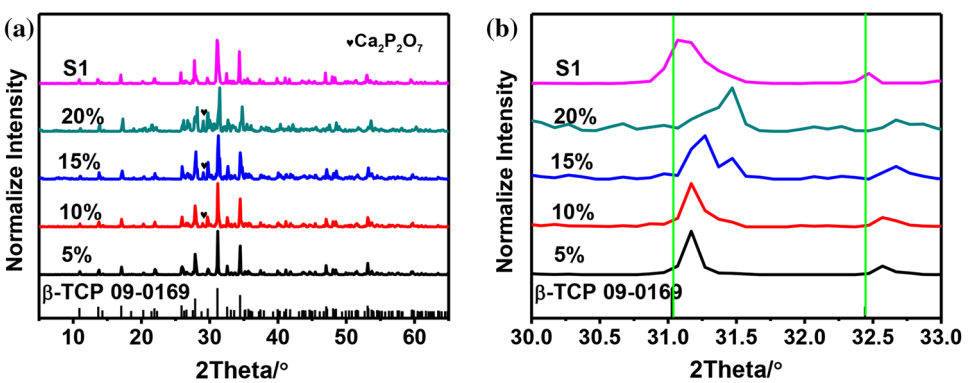

Figure 3 **a** XRD patterns of the β-TCP/BG scaffolds with BG content varying from 5 wt% to 20 wt%, **b** corresponding enlarged patterns in the 30.0–33.0° range.

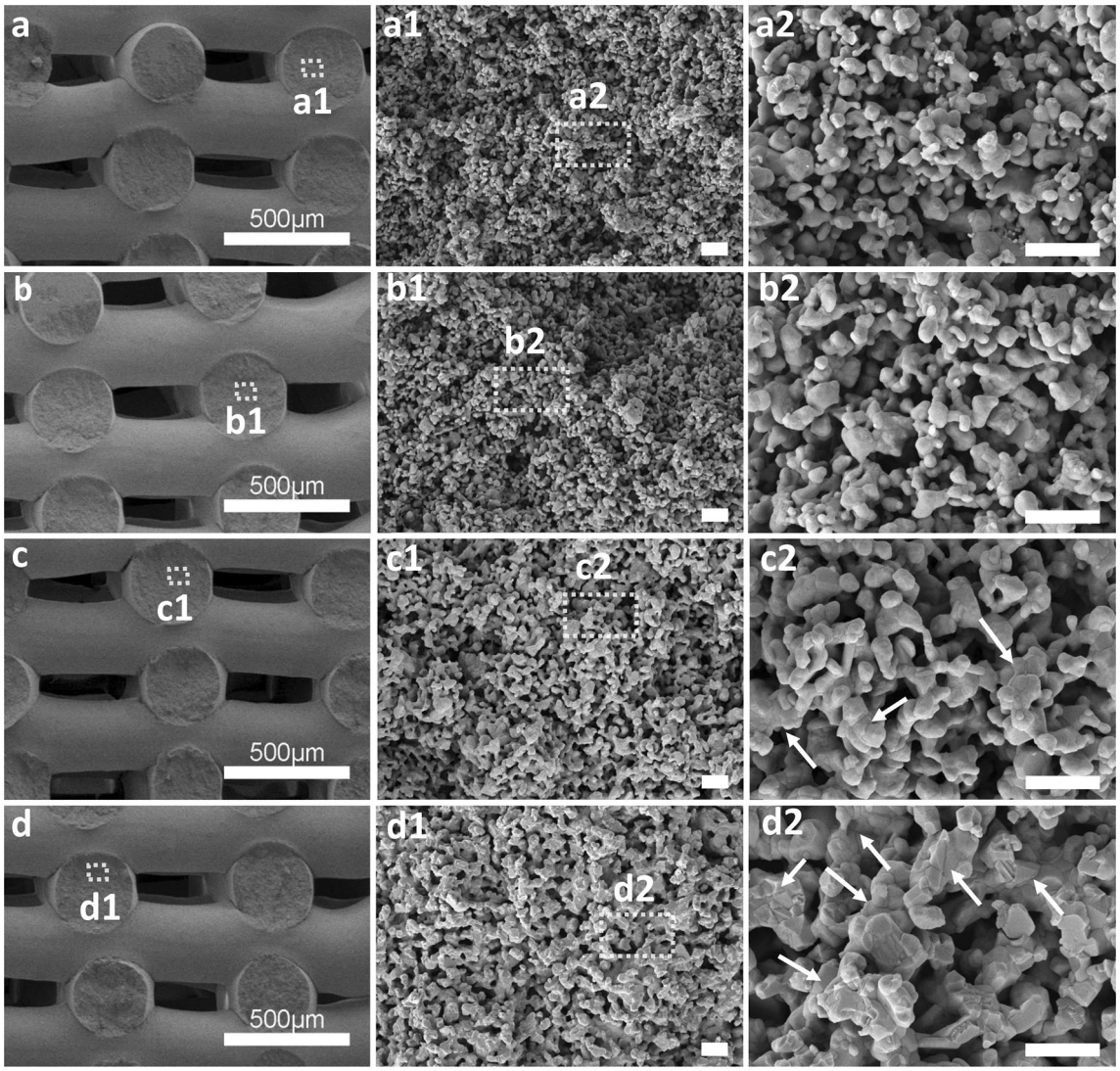

Figure 4 Cross-sectional microstructures (SEM observation) of β-TCP/BG5, β-TCP/BG10, β-TCP/BG15, β-TCP/BG20 scaffolds (**a**–**d**). The scale bar in the figures represents 2 μm.

reasonable that as shown in Table 1, the pure β-TCP ceramics scaffolds sintered at 1100 °C (S1) exhibited higher linear shrinkage of 15.32% in the x and y directions, the β-TCP/BG20 scaffolds sintered at 800 °C (S2) showed a shrinkage rate of 9.35%, and the β-TCP/BG scaffolds sintered at 710 °C showed a smaller shrinkage rate of less than 6% in the x and y directions. Reasonably, the addition of bioglass can decrease the sintering temperature of β-TCP ceramic scaffolds, and the use of an appropriate sintering temperature can reduce the shrinkage rate and guarantee the sintering mechanical structure.

Table 1 Shrinkage rate of the scaffolds

Shrinkage (%)	5%	10%	15%	20%	S1	S2
x–y direction	3.01	3.56	5.35	5.89	9.35	15.32
z direction	3.23	3.65	5.45	6.01	9.48	15.52

Mechanical properties of the scaffolds

To investigate the effect of bioglass on the mechanical property of the β-TCP ceramic scaffolds, we examined the samples using a universal mechanical testing instrument, and the obtained results are shown in Fig. 5. The β-TCP/BG20 scaffolds showed a better

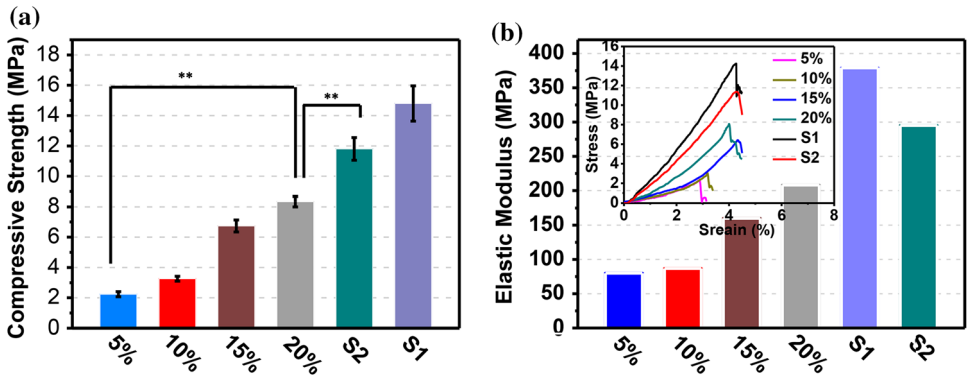

Figure 5 **a** Compressive strength of the β-TCP/BG scaffolds with bioglass addition varying from 5 to 20% and S1, S2, **b** elastic modulus of the β-TCP/BG scaffolds with bioglass addition varying from 5 to 20% and S1, S2.

compressive strength of 8.34 MPa and an elastic modulus of 208.5 MPa than the scaffolds with less bioglass addition. The compressive strength of the β-TCP/BG15 scaffold was 6.74 MPa, and the elastic modulus was 160 MPa, satisfying the mechanical properties requirement of cancellous bone repair [47]. A significant correlation between the content of bioglass and the increase in the scaffolds' compressive strength was observed. It is important to note that the S1 and S2 scaffolds exhibited superior mechanical properties due to the higher shrinkage and compact dense internal structure.

Degradation behavior of β-TCP/BG scaffolds in vitro

To investigate the effect of bioglass on the degradability of ceramic scaffolds, we measured the weight loss of the scaffolds after soaking them in a Tris–HCl buffer for different time periods. The obtained weight loss and pH change data are shown in Fig. 6. Generally, the β-TCP/BG20 scaffold exhibited better degradability than other group. The weight losses of the β-TCP/BG20, β-TCP/BG15, β-TCP/BG10, β-TCP/BG5 and S1 scaffolds after immersion for 35 days were 6.82%, 4.38%, 3.189%, 2.68% and 2.28%, respectively. The weight loss of the S1 scaffolds was consistent with the result for the pure β-TCP porous scaffold (< 2.5%) reported elsewhere [19, 47]. It is noteworthy that the weight loss rate of the β-TCP/BG20 scaffolds was 2.99 times greater than that of S1 and that the corresponding calculated result for the β-TCP/BG15 scaffolds was 1.92 times than that of S1. These results demonstrated the remarkable improvement in the degradation performance of the β-TCP scaffolds obtained by the addition of bioglass. Figure 6c, e, f shows the surface morphology changes of the degraded β-TCP/BG20 ceramic scaffold after immersion for 14 days in a PBS buffer. SEM observation revealed a large change in the surface morphology of the β-TCP/BG20 ceramic scaffold from that of the S1 scaffold. Many large and small crater-shaped morphology features were observed on the surface of the filaments of the β-TCP/BG20 scaffold. Moreover, the degradation and disappearance of the bonding sites between the particles is observed in Fig. 6f, as indicated by white arrows. In particular, there was no significant change in the pH value beyond the early slight increase that could be attributed to the existence of $Ca_2P_2O_7$.

Cell proliferation assay

As shown in Fig. 7, an MTT assay was used to investigate the influence of the bioglass addition on the biocompatibility of the β-TCP ceramic scaffold. Compared to the control group, β-TCP/BG ceramic scaffolds showed higher OD values and displayed no visible cytotoxicity. In particular, the β-TCP/BG15 scaffolds were observed to be more beneficial for the growth of MC3T3-E1 preosteoblasts than other group. It was easily found that there was a significant promotion effect of β-TCP/BG on the MC3T3-E1 preosteoblasts proliferation that showed a corresponding relationship with the added bioglass content. The greater proportion of the $Ca_2P_2O_7$ component and the higher pH value in the early stage contribute to the decrease in the OD value of β-TCP/BG20.

Conclusions

In this study, a β-TCP powder with an average particle size of 600 nm and a Na_2O–CaO–MgO–P_2O_5 bioglass powder with an average particle size of

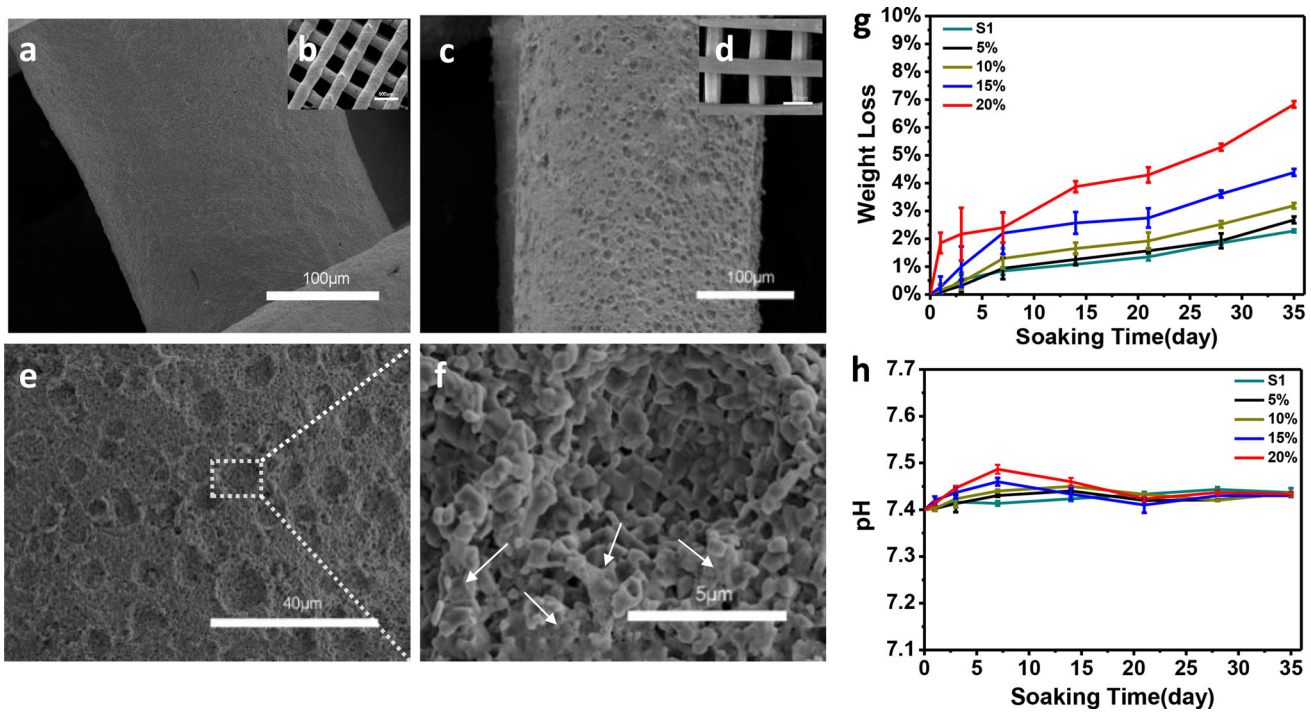

Figure 6 Surface morphology of β-TCP/BG20 scaffold before (**a**, **b**) and after soaking for 14 days in a Tris–HCl buffer (**c**–**f**), the weight loss (**g**), pH value variation (**h**) of scaffolds after being soaked in a Tris–HCl buffer for different time periods.

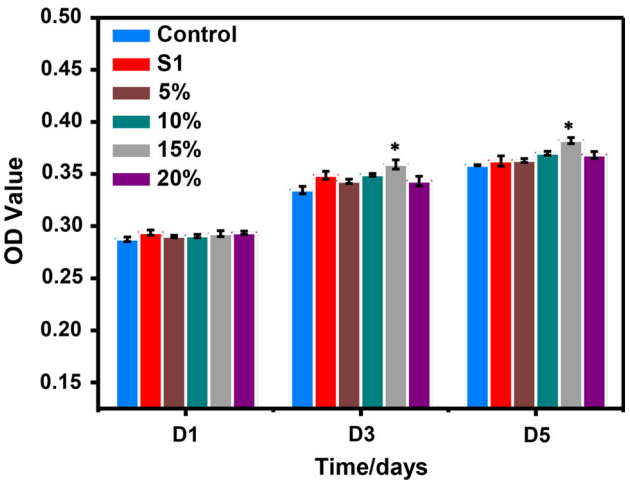

Figure 7 MTT results of the proliferation of MC3T3-E1 preosteoblasts. A culture medium (100 μL) containing the MC3T3-E1 preosteoblasts was exposed to the scaffolds for 1, 3 and 5 days. The data are represented as the mean ± SD, $n = 3$. $^{*}p < 0.05$, $^{**}p < 0.01$ versus control.

1.3 μm were prepared. Additionally, porous β-TCP/BG scaffolds with uniform ~ 400 μm macropores were fabricated by 3D printing and were sintered at 710 °C. The bioglass played a decisive role in the enhancement of mechanical strength, degradability and biocompatibility. Moreover, the reinforced β-TCP/BG porous ceramic scaffolds showed a compressive strength of 8.34 MPa and an elastic modulus of 208.5 MPa. The degradation rate was increased by a factor of 2.99. The MTT assay showed a significant promotion of β-TCP/BG15% on the proliferation of the MC3T3-E1 osteoblast cells. Na_2O–CaO–MgO–P_2O_5 bioglass-reinforced β-TCP porous ceramic scaffold shows great potential for application in bone tissues repair.

Acknowledgements

This work was supported by the grant from the National Key Research and Development Program of China (2018YFB1105500, 2016YEC1101605, 2016YFB1101302 and 2017YFC1103800), the National Natural Science Foundation of China (No. 51772233) and the Application Foundation and Front research program of Wuhan (No. 2018010401011273).

Electronic supplementary material: The online version of this article (https://doi.org/10.1007/s10853-019-03632-3) contains supplementary material, which is available to authorized users.

References

[1] Bergmann C, Lindner M, Zhang W et al (2010) 3D printing of bone substitute implants using calcium phosphate and bioactive glasses. J Eur Ceram Soc 30:2563–2567

[2] Vacanti JP, Langer R (1999) Tissue engineering: the design and fabrication of living replacement devices for surgical reconstruction and transplantation. The Lancet 354:S32–S34

[3] Ratner BD, Hoffman AS, Schoen FJ et al (2004) Biomaterials science: an introduction to materials in medicine. Elsevier, Amsterdam

[4] Murphy CM, Haugh MG, O'Brien FJ (2010) The effect of mean pore size on cell attachment, proliferation and migration in collagen–glycosaminoglycan scaffolds for bone tissue engineering. Biomaterials 31:461–466

[5] Rouwkema J, Rivron NC, van Blitterswijk CA (2008) Vascularization in tissue engineering. Trends Biotechnol 26:434–441

[6] LeGeros RZ, Lin S, Rohanizadeh R et al (2003) Biphasic calcium phosphate bioceramics: preparation, properties and applications. J Mater Sci Mater Med 14:201–209

[7] Sánchez-Salcedo S, Arcos D, Vallet-Regí M (2008) Upgrading calcium phosphate scaffolds for tissue engineering applications. Key Eng Mater 377:19–42

[8] Flautre B, Descamps M, Delecourt C et al (2001) Porous HA ceramic for bone replacement: role of the pores and interconnections—experimental study in the rabbit. J Mater Sci Mater Med 12:679–682

[9] Klein C, de Groot K, Chen W et al (1994) Osseous substance formation induced in porous calcium phosphate ceramics in soft tissues. Biomaterials 15:31–34

[10] Orlovskii VP, Komlev VS, Barinov SM (2002) Hydroxyapatite and hydroxyapatite-based ceramics. Inorg Mater 38:973–984

[11] Daculsi G, Laboux O, Malard O, Weiss P (2003) Current state of the art of biphasic calcium phosphate bioceramics. J Mater Sci Mater Med 14:195–200

[12] Le Huec JC, Schaeverbeke T, Clement D et al (1995) Influence of porosity on the mechanical resistance of hydroxyapatite ceramics under compressive stress. Biomaterials 16:113–118

[13] Kwon S-H, Jun Y-K, Hong S-H, Kim H-E (2003) Synthesis and dissolution behavior of β-TCP and HA/β-TCP composite powders. J Eur Ceram Soc 23:1039–1045

[14] Wang Z, Guo Z, Bai H et al (2013) Clinical evaluation of beta-TCP in the treatment of lacunar bone defects: a prospective, randomized controlled study. Mater Sci Eng C 33:1894–1899

[15] Lu Z, Zreiqat H (2010) Beta-tricalcium phosphate exerts osteoconductivity through α2β1 integrin and down-stream MAPK/ERK signaling pathway. Biochem Biophys Res Commun 394:323–329

[16] Wiltfang J, Merten HA, Schlegel KA et al (2002) Degradation characteristics of α and β tri-calcium-phosphate (TCP) in minipigs. J Biomed Mater Res 63:115–121

[17] Chappard D, Guillaume B, Mallet R et al (2010) Sinus lift augmentation and beta-TCP: a microCT and histologic analysis on human bone biopsies. Micron 41:321–326

[18] Houmard M, Fu Q, Genet M et al (2013) On the structural, mechanical, and biodegradation properties of HA/beta-TCP robocast scaffolds. J Biomed Mater Res B Appl Biomater 101:1233–1242

[19] Oonishi H, Oomamiuda H (2016) Degradation/resorption in bioactive ceramics in orthopaedics. In: Murphy W, Black J, Hastings G (eds) Handbook of biomaterial properties. Springer, New York, pp 495–507

[20] Hench LL, Polak JM (2002) Third-generation biomedical materials. Science 295:1014–1017

[21] Deng C, Yao Q, Feng C et al (2017) 3D printing of bilineage constructive biomaterials for bone and cartilage regeneration. Adv Funct Mater 27:1703117

[22] Handschel J, Wiesmann HP, Stratmann U et al (2002) TCP is hardly resorbed and not osteoconductive in a non-loading calvarial model. Biomaterials 23:1689–1695

[23] Chen QZ, Thompson ID, Boccaccini AR (2006) 45S5 Bioglass®-derived glass–ceramic scaffolds for bone tissue engineering. Biomaterials 27:2414–2425

[24] Oonishi H, Kushitani S et al (1997) Particulate bioglass compared with hydroxyapatite as a bone graft substitute. Clin Orthop Relat Res 334:316–325

[25] Xynos ID, Edgar AJ, Buttery LDK et al (2001) Gene-expression profiling of human osteoblasts following treatment with the ionic products of Bioglass® 45S5 dissolution. J Biomed Mater Res 55:151–157

[26] Rezwan K, Chen QZ, Blaker JJ, Boccaccini AR (2006) Biodegradable and bioactive porous polymer/inorganic composite scaffolds for bone tissue engineering. Biomaterials 27:3413–3431

[27] Xynos ID, Edgar AJ, Buttery LDK et al (2000) Ionic products of bioactive glass dissolution increase proliferation of human osteoblasts and induce insulin-like growth factor II mRNA expression and protein synthesis. Biochem Biophys Res Commun 276:461–465

[28] Dai C, Guo H, Lu J et al (2011) Osteogenic evaluation of calcium/magnesium-doped mesoporous silica scaffold with incorporation of rhBMP-2 by synchrotron radiation-based μC. Biomaterials 32:8506–8517

[29] Feng B, Jinkang Z, Zhen W et al (2011) The effect of pore size on tissue ingrowth and neovascularization in porous

bioceramics of controlled architecture in vivo. Biomed Mater 6:015007
[30] Ramay HR, Zhang M (2004) Biphasic calcium phosphate nanocomposite porous scaffolds for load-bearing bone tissue engineering. Biomaterials 25:5171–5180
[31] Ratner BD, Hoffman AS, Schoen FJ et al (2004) Biomaterials science: an introduction to materials in medicine. Elsevier, Amsterdam
[32] Karageorgiou V, Kaplan D (2005) Porosity of 3D biomaterial scaffolds and osteogenesis. Biomaterials 26:5474–5491
[33] Wu S, Liu X, Yeung KWK (2014) Biomimetic porous scaffolds for bone tissue engineering. Mater Sci Eng R 80:1–36
[34] Leukers B, Gülkan H, Irsen SH et al (2005) Hydroxyapatite scaffolds for bone tissue engineering made by 3D printing. J Mater Sci Mater Med 16:1121–1124
[35] Inzana JA, Olvera D, Fuller SM et al (2014) 3D printing of composite calcium phosphate and collagen scaffolds for bone regeneration. Biomaterials 35:4026–4034
[36] Wu C, Fan W, Zhou Y et al (2012) 3D-printing of highly uniform CaSiO 3 ceramic scaffolds: preparation, characterization and in vivo osteogenesis. J Mater Chem 22:12288–12295
[37] Castilho M, Moseke C, Ewald A et al (2014) Direct 3D powder printing of biphasic calcium phosphate scaffolds for substitution of complex bone defects. Biofabrication 6:015006
[38] Neufurth M, Wang X, Wang S et al (2017) 3D printing of hybrid biomaterials for bone tissue engineering: calcium-polyphosphate microparticles encapsulated by polycaprolactone. Acta Biomater 64:377–388
[39] Cox SC, Thornby JA, Gibbons GJ et al (2015) 3D printing of porous hydroxyapatite scaffolds intended for use in bone tissue engineering applications. Mater Sci Eng, C 47:237–247
[40] Pei X, Ma L, Zhang B et al (2017) Creating hierarchical porosity hydroxyapatite scaffolds with osteoinduction by three-dimensional printing and microwave sintering. Biofabrication 9:045008
[41] Xu W, Xu C, Yi J, Dai H (2018) The effect of different hydroxyapatite microparticles on the osteogenic differentiation of MC3T3-E1 preosteoblasts. J Mater Chem B 6:5234–5242
[42] Brunner TJ, Grass RN, Bohner M et al (2007) Effect of particle size, crystal phase and crystallinity on the reactivity of tricalcium phosphate cements for bone reconstruction. J Mater Chem 17:4072–4078
[43] Lee S-H, Kochawattana S, Messing GL et al (2006) Solid-state reactive sintering of transparent polycrystalline Nd:YAG ceramics. J Am Ceram Soc 89:1945–1950
[44] Dunne M, Corrigan O, Ramtoola Z (2000) Influence of particle size and dissolution conditions on the degradation properties of polylactide-co-glycolide particles. Biomaterials 21:1659–1668
[45] Lin K, Chang J, Liu Z, Zeng Y, Shen R (2009) Fabrication and characterization of 45S5 bioglass reinforced macroporous calcium silicate bioceramics. J Eur Ceram Soc 29:2937–2943
[46] Wang S, Falk MM, Rashad A et al (2011) Evaluation of 3D nano–macro porous bioactive glass scaffold for hard tissue engineering. J Mater Sci Mater Med 22:1195–1203
[47] Chen L, Deng C, Li J et al (2019) 3D printing of a lithium-calcium-silicate crystal bioscaffold with dual bioactivities for osteochondral interface reconstruction. Biomaterials 196:138–150